Jahn, S., Schmidt, C. (2010): Speciation in Aqueous MgSO4 Fluids at High Pressures and High Temperatures from ab Initio Molecular Dynamics and Raman Spectroscopy. - Journal of Physical Chemistry B, 114, 47, 15565-15572

DOI: 10.1021/jp101749h

Speciation in aqueous $MgSO_4$ fluids at high pressures and high temperatures from *ab initio* molecular dynamics and Raman spectroscopy

Sandro Jahn* and Christian Schmidt

GFZ German Research Centre for Geosciences, Section 3.3, Telegrafenberg, 14473 Potsdam, Germany

E-mail: jahn@gfz-potsdam.de

*To whom correspondence should be addressed

Abstract

Ab initio molecular dynamics simulations and *in situ* Raman spectroscopy are used to study the speciation in two molal aqueous $MgSO_4$ solutions at high pressures, P, and temperatures, T. While at ambient conditions the fluid is dominated by dissociated SO_4^{2-}(aq) ions and solvent separated ion pairs, ion association strongly increases with increasing temperature and pressure along an 1.33 g/cm^3 isochore. At $T = 450$ °C and $P = 1.4$ GPa, the ν_1-SO_4^{2-} Raman band is well described by three Gaussian+Lorentzian components of about equal intensity with peaks at about 980, 995 and 1005 cm^{-1}. Analysis of the simulations, however, indicates the coexistence of more than three species, including dissociated SO_4^{2-}(aq) ions, contact and triple ion pairs as well as larger complexes. In addition, the sulfate groups may be bonded to Mg as monodentate or bidentate ligands. The frequencies of the associated species seem to depend mainly on the type and number of Mg-SO_4 bonds. We interpret the two rather broad high-frequency Raman components as a single 'Mg-SO_4 contact' component with variable frequency distribution. As a consequence, the ν_1-SO_4^{2-} Raman band provides only information on the molecular environment of the sulfate group, i.e. individual species cannot be resolved. At fluid densities less than about 1.2 g/cm^3 and temperatures above 400 °C, the formation of HSO_4^-(aq) containing species is observed in both simulations and experiments, which may be accompanied by a change in pH and electrical conductivity.

Introduction

The binary H_2O-$MgSO_4$ is one of the most important systems to model natural aqueous fluids. Magnesium sulfate is the second most abundant solute in Earth's seawater, and sulfate is very common in aqueous fluids and melts in the lithosphere[1]. Under oxidizing conditions, sulfate can be transported to great depth (at least to ∼40 km) in subduction zones and released into the fluid phase upon slab dehydration[2]. In addition, there is growing evidence that $MgSO_4$ plays a very important role in extraterrestrial aqueous environments. It is long known that magnesium sulfates are by far the most abundant water-soluble low-temperature aqueous alteration products in car-

bonaceous chondrites[3]. Hydrated magnesium sulfates have been found on the surfaces of Mars[4], and Europa[5]. Galileo spacecraft magnetometric measurements indicated an electrically conductive layer in the near-surface interior of the Jupiter moon Europa, interpreted as subsurface ocean with Mg^{2+} and SO_4^{2+} as dominant dissolved ions[6].

Aqueous $MgSO_4$ solutions have been studied extensively at ambient pressure, P, as a function of temperature, T. In an early work, Noyes *et al.*[7] related the electrical conductivity of aqueous $MgSO_4$ fluids to their degree of ionization. For a 0.01 molal solution, the electrical conductivity initially increases from ambient T to about $100-150$ °C and is reduced again at higher temperatures[8]. Close to ambient conditions, a maximum in the specific conductivity was observed at a concentration corresponding to a 1.7 molal solution[9].

Studies using ultrasonic absorption and dielectric relaxation spectroscopies have shown the simultaneous existence of different associated species[10,11], which according to the association model of Eigen and Tamm[10] are the double solvent separated ion pair (2SIP), $Mg(H_2O)_2SO_4$(aq), the solvent separated ion pair (SIP), $Mg(H_2O)SO_4$(aq), and the contact ion pair (CIP), $MgSO_4$(aq). For concentrated solutions (>1 molal), triple ions (TI), e.g. $MgSO_4Mg^{2+}$(aq), or more aggregated species are suggested[11]. Based on information from dielectric relaxation spectroscopy, the concentration of TIs increases strongly with temperature and concentration, and that of CIPs increases steadily with the total solute concentration at 5 and 25 °C and passes through a maximum at ∼1.8 molal at 45 °C and ∼1.4 molal at 65 °C, due to increasing TI formation[12]. The concentrations of 2SIPs and SIPs generally decrease with temperature and go through maxima at ∼0.1 and ∼0.5 molal[12].

Furthermore, temperature and concentration dependent changes of the symmetric stretching mode of sulfate ($\nu_1-SO_4^{2-}$) in Raman spectra of $MgSO_4$ solutions have been related to the coexistence of different sulfate species[13–17]. Although the interpretation of the observed spectra has been somewhat controversial, particularly on the assignment of the $\nu_1-SO_4^{2-}$ band component at ∼995 cm^{-1} to CIPs[14], most authors agree that these changes are due to increasing concentrations of more associated species, including bidentate ligands, triple ions and larger clusters[15,17]. The

Raman data also suggest the dominance of CIPs at higher temperature[17], which is in agreement with the relaxation spectroscopic studies mentioned above. The interpretation of the vibrational spectra was accompanied by *ab initio* simulation studies on hydrated clusters[18–20].

However, much less is known about $MgSO_4$ in aqueous fluids at high P and T as present in planetary interiors. Ritzert and Franck[8] studied 0.01 molal $MgSO_4$ fluids at densities between 0.8 and 1.2 g/cm^3 and temperatures from ambient to 317 °C. They found generally higher electrical conductivity with increasing pressure at constant T, but this ceased at densities above 1.1 g/cm^3, at least along isotherms to 87 °C. From an exploratory Raman spectroscopy study of an 0.5 molal $MgSO_4$ solution up to 1.1 GPa and 500 °C, Frantz et al.[21] conclude increasing $MgSO_4$ association with increasing P and T along an isochore corresponding to a density of about 1.0 g/cm^3.

The distribution of sulfate species at high P, T and $MgSO_4$ concentrations, x, in these solutions is still largely unknown. Their determination requires not only *in situ* measurements but also reliable molecular modeling for interpretation of the experimental data. Here we combine both approaches to address this issue. While the simulations help to identify different species and their stability as a function of P and T, the experiments provide quantitative information on their distribution. Experimental methods that may provide direct or indirect information on the structure of aqueous fluids include optical spectroscopy[21] as well as x-ray and neutron scattering techniques[22]. Raman spectroscopy is the experimental method of choice to study speciation in fluids at extreme conditions since it is element specific and sensitive enough to cope with the small sample volumes in high $P-T$ optical cells[21,23].

Regarding different methods of molecular modeling, a reasonable compromise between accuracy and efficiency has to be made. Accurate vibrational frequencies of the sulfate group have been obtained from static cluster calculations of different species using quantum chemical methods[18–20]. Those frequencies may be representive of the fluid close to ambient conditions but they are not directly applicable to extreme conditions. For a quantitative analysis of speciation, a sufficiently large set of molecular configurations has to be sampled. For aqueous NaCl solutions, speciation was evaluated from long classical molecular dynamics simulations at ambient[24] and

supercritical[25] conditions. However, it was shown recently[26] that both the binding free energy of NaCl in solution and the Na–Cl distance in SIPs vary considerably between popular classical force fields and more accurate density-functional theory (DFT)[27,28] based calculations. Since $MgSO_4$ solutions are chemically more complex than NaCl solutions, their classical force fields are expected to be even less reliable, especially towards extreme conditions of P and T. We therefore chose an *ab initio* DFT-based approach to perform molecular dynamics simulations. The latter is computationally much more expensive than classical force field calculations and hence restrictions on system size and total simulation time are more severe. However, the kinetics of speciation changes is reasonably fast at the high temperatures of interest here. Another advantage of the quantum mechanical method chosen here over classical potentials is the ability to predict chemical reactions (e.g. hydrolysis) and hence the formation of new species without need of explicit parameterization.

Methods

Ab initio molecular dynamics simulations

The *ab initio* molecular dynamics simulations are performed using the Car-Parrinello technique[29] as implemented in the CPMD code[30]. The system consists of 120 water and four $MgSO_4$ molecules, which adds up to a total of 384 atoms. Such a relatively large simulation cell is needed to represent an about two molal solution and to allow for ion pairing, for which at least a few molecules of the solute need to be present. The calculations are performed using the BLYP exchange correlation functional[31,32] in conjunction with Goedecker-type pseudopotentials[33]. The Kohn-Sham orbitals are expanded in plane-waves up to an energy of 70 Ry. For the Car-Parrinello molecular dynamics, a fictitious electron mass of 600 a.u. and a time step of 0.12 fs are used. The CPMD simulations are performed in the NVT ensemble (constant number of particles, volume and temperature). The temperature is controlled by a Nosé-Hoover chain thermostat[34,35].

The initial structure with a fluid density of 0.75 g/cm^3 is taken from a classical molecular dynamics simulation of pure H_2O using the SPC/E potential, to which the ions are added. This

configuration is then annealed in a CPMD simulation for 8 ps at a temperature of 727 °C. Starting configurations for simulations at higher densities are subsequently produced by rescaling the simulation cell and atomic positions of the previous lower density simulation. At each volume, short equilibration runs of $3-4$ ps are made before production runs of at least 10 ps are started and new higher density configurations are produced. The highest fluid density of this study is 1.50 g/cm^3. The final configurations of the 727 °C production runs are then cooled subsequently to 527, 327 and 227 °C keeping the cell volume constant. Again, short equilibration runs are performed at each temperature before production runs are started or the temperature is reduced further.

Raman spectroscopy

An externally heated Bassett-type hydrothermal diamond-anvil cell (HDAC)[36] equipped with type Ia ultra-low fluorescence grade diamond anvils (culet diameter 0.9 mm) was used as optical cell. The temperature in the sample chamber of the HDAC was measured using K-type thermocouples attached to the diamonds, and calibrated based on the $\alpha-\beta$ quartz transition temperature (574 °C at 0.1 MPa) and the triple point of H_2O (0.01 °C, 0.6 kPa). The power input to the resistive heaters (NiCr coils around the tungsten carbide seats of the diamonds) was controlled using Eurotherm 2408 temperature controllers, which held the set temperature within $\pm$0.2 °C during spectra recording.

A piece of natural quartz and a 2.0 molal $MgSO_4$ solution were loaded into the HDAC sample chamber, which consisted of a hole (initial diameter 500 μm) in an iridium gasket separating the anvils. Because of water evaporation during loading, the actual $MgSO_4$ concentration was somewhat higher in the sealed sample chamber. A solute concentration of about 2.2$\pm$0.1 molal was obtained from spectral parameters of the ν_1-SO_4^{2-} Raman band (integrated intensity percentage of the band component at $\sim$995 cm^{-1}, Raman shift and full width at half maximum of the component at $\sim$980 cm^{-1}) measured at 22 °C and 0.38 GPa. These parameters were calibrated using measurements on $MgSO_4$ solutions in the HDAC, the concentrations of which were constrained from the vapor-saturated liquidus temperature. The pressure was determined from the calibrated

frequency shift of the 464 cm^{-1} Raman line of quartz (Schmidt and Ziemann[37], equations (2) and (3) therein), with a random error of about 25 MPa.

The 2.2 molal solution was heated along an isochore from 22 °C, 0.38 GPa to 450 °C, 1.4 GPa (Figure 1). These $P-T-x$ conditions correspond to a fluid density of 1.33 g/cm[3][3]. Unpolarized Raman spectra of the solution in the region of the sulfate symmetric stretching mode (ν_1-SO_4^{2-}) and of quartz were recorded at several temperatures. Along this heating path, the fluid was supersaturated with respect to kieserite (monoclinic $MgSO_4{\cdot}H_2O$) at most conditions, except at 22 °C and, possibly, at 100 °C[3]. At 450 °C, the pressure decreased slightly with time, the surface of the quartz chip appeared corroded, and unidentified small precipitates formed. Further heating to 500 °C caused rapid growth of a kieserite crystal, coupled with a substantial decrease in pressure from 1.4 to 0.9 GPa (Figure 1). Upon cooling, this crystal continued to grow at 400 °C, but started to dissolve at T$\leq$300 °C. Sulfate crystals were still present after cooling to 22 °C, vapor pressure.

The Raman spectra were acquired in backscattering geometry using a HORIBA Jobin Yvon LabRAM HR800 UV-Vis Raman microprobe (gratings 1800 lines/mm, focal length 800 mm, confocal pinhole aperture 100 μm, objective Nikon MPlan SLWD 40x, excitation by 488.0 nm line from Ar^+ laser). The laser interference filter was removed to record plasma lines for wavenumber calibration. The laser power at the source was 407$\pm$1 mW. This corresponded to a power at the entrance of the optical cell of about 66 mW, and was low enough to avoid laser heating of the sample. Raman spectra of the solution were collected with 20 (some spectra 5 or 10) accumulations of 20 s each, those of quartz with 10 accumulations of 15 s each. Nominal focal point positions in the fluid were 15 to 30 μm below the upper sample chamber surface to obtain comparable integrated intensities of Raman bands[23,38]. Spectra fitting was done using a linear baseline, a symmetric shape (Gaussian-Lorentzian sum (area) model) for the ν_1-SO_4^{2-} components[17] and the asymmetric model Pearson IV for Raman lines of quartz and plasma lines[23,37].

Results

Solvent structure from CPMD

Changes in the solvent structure with pressure at the highest temperature (727 °C) are similar to those discussed in a previous paper on aqueous LiF solutions[39]. Intermolecular O-H distances and oxygen-oxygen distances decrease with increasing pressure. A shoulder in the O-H radial distribution function, $g_{OH}(r)$ at a distance r of about 2 Å indicates the presence of some hydrogen bonding. There is, however, strong overlap with the non-hydrogen bonded O-H peak at about 3 Å. Analysis of the dynamics of the hydrogen bonds reveals very short lifetimes of no more than 0.1 ps. The nearest neighbor coordination number of oxygen by other oxygen ions increases from 9.0 at the lowest pressure ($\rho = 0.75$ g/cm^3) to about 12.5 at a density of 1.2 g/cm^3. Then, it remains constant towards higher densities, which indicates a close packing of oxygen ions. With decreasing temperature, the nearest neighbor oxygen-oxygen distance becomes shorter. As in the aqueous LiF system[39], there is a change in the slope of the oxygen-oxygen distance at high fluid densities (here between 1.2 and 1.4 g/cm^3, see Figure 2). The first intermolecular peak in $g_{OH}(r)$ that is related to hydrogen bonding becomes more pronounced at lower temperature and is observed between 1.7 (highest density) and 2.0 Å (lowest density).

Some hydrolysis is observed especially at lower densities (see Figure 3). Both proton and hydroxide ions from dissociation of H_2O molecules do not exist as free species but attach quickly to SO_4^{2-} and Mg^{2+} ions to form HSO_4^- and $MgOH^+$ containing complexes (see Figure 4).

Solute speciation from CPMD

During the course of the simulations a variety of solute species is observed, some of which are illustrated in Figure 4. As mentioned above, hydrolysis leads to the formation of HSO_4^- and $MgOH^+$ containing complexes, especially at densities below 1.1 g/cm^3. At the lowest density (0.75 g/cm^3), two Mg ions cluster in a $SO_4(MgOH)_2$(aq) complex with short Mg-Mg distance (3.0 to 3.8 Å). At the highest densities, part of the solutes is dissociated into Mg^{2+}(aq) and SO_4^{2-}(aq) ions. The

dominant species at densities above 1.0 g/cm^3 are, however, contact ion pairs $MgSO_4$(aq), triclusters and short chains of $MgSO_4MgSO_4$(aq). In these complexes, SO_4^{2-} acts as both monodentate or bidentate ligand. The distinction between the latter is apparent in the $g_{MgS}(r)$ radial distribution function (see Figure 5). Especially at high temperatures, changes in the speciation are frequent even on the short picosecond time scale of the CPMD simulations. As a result, a distribution of mono- and bidentate ligands is observed over the whole density range. This distribution shows a shift from predominantly bidentate towards predominantly monodentate sulfate ligands with increasing fluid density (Figure 5).

The distribution of vibrational frequencies of the four sulfur atoms is obtained from the power spectra $z^S(\nu)$ of the velocity autocorrelation functions[40]. Note that these spectra contain all frequencies that involve motions of the sulfur atoms and that they are not directly comparable to the Raman spectra presented below, which are related to changes in the polarizability. Therefore, only the peak frequencies are compared and discussed but not the spectral shapes. As an example, the $z^S(\nu)$ for the simulations at $T = 272$ °C and $\rho = 1.10$ g/cm^3 are shown in Figure 6. In this case, three different aqueous species are identified. The first is a $(SO_4)Mg(SO_4)^{2-}$(aq) tricluster where the two sulfate groups are both bonded to a single Mg. The corresponding sulfur frequency spectra are peaked at 988 and 967 cm^{-1}. Both sulfate groups act predominantly as monodentate ligands, but in the course of the simulation they are temporarily transformed into bidentate ligands (10 % and 40 % of the total simulation time, respectively). The second species is a $Mg_2(SO_4)(MgOH)^{3+}$(aq) complex, that was not observed in simulations at other densities. The spectral weight of this complex is slightly shifted to higher frequencies (maximum at 1005 cm^{-1}). Finally, an HSO_4^-(aq) complex with a considerably higher peak frequency of 1090 cm^{-1} is observed.

Figure 7 gives the distribution of species and their vibrational frequencies. Only the maxima of those $z^S(\nu)$ are shown that clearly correspond to individual species, i.e. the frequency maxima of sulfate ions that change their speciation during the simulation are omitted. The HSO_4^- containing species are clearly concentrated in the lower density region at distinctly higher frequencies com-

pared to those of SO_4^{2-} containing species. Even though the scatter in the frequencies of the latter is large, CIPs with bidentate ligands appear to have higher frequencies than monodentate CIPs. Adding a second (or third) Mg neighbor to a SO_4^{2-} group may also increase the frequency slightly (see also Figure 6).

The frequency changes between the different species may be related to deformations of the SO_4 tetrahedra. The fully hydrated SO_4(aq) complex resembles in average a perfect tetrahedron with O-S-O bond angles close to 109.5° and a mean bond length of 1.52 Å. When a contact ion pair is formed, the S-O bond length of the oxygen bonded to a Mg is slightly increased to about 1.54 Å. The other S-O bond lengths should decrease accordingly but this could not be resolved due to statistical fluctuations. Changes in the bond angles are significant but smaller than 2°. Much larger deviations are observed for the HSO_4^-(aq) complex. The mean S-O(-H) bond length is increased to 1.66 Å, while the other S-O distances are decreased to 1.49-1.50 Å. Mean O-S-O(-H) bond angles are observed between 104° to 107° while the remaining O-S-O bond angles range between 112° and 113°.

Finally, the mean Mg coordination by oxygens is shown in Figure 8. It increases almost linearly with density in the range considered here from dominantly 5-fold to 6-fold coordination. With decreasing temperature at constant volume, the coordination appears to increase slightly but the low-T results are much more scattered, which indicates that in this case longer simulation times are needed to provide reliable averages.

Raman spectra

Figure 9 shows Raman spectra of the 2.2 molal $MgSO_4$ solution obtained at several temperatures along the isochoric heating path. Below 150 °C, the Raman band shape in the ν_1-SO_4^{2-} region was accurately described by two Gaussian+Lorentzian components centered at $\sim$995 cm^{-1} and $\sim$980 cm^{-1}. However, significant nonstatistical residuals were present in the high frequency region of the ν_1-SO_4^{2-} Raman mode at temperatures above 150 °C. Excellent fits for the high temperature spectra were obtained by adding a third Gaussian+Lorentzian component centered at $\sim$1005 cm^{-1}.

The integrated intensity percentage of these three components of the ν_1-SO_4^{2-} band is shown in Figure 10 along the isochoric heating path, assuming equal Raman scattering cross sections of the individual components. The proportion of the component at ~980 cm^{-1} generally decreases with temperature, which is coupled with an increase in the fraction of the component at ~995 cm^{-1}. At about 350 °C, there appears to be a minimum in the fraction of the ~980 cm^{-1} component. The ~995 cm^{-1} component shows a maximum at about 300 °C (Figure 10). These temperatures roughly coincide with the observed solubility minimum of kieserite along the cooling path. The component at ~1005 cm^{-1} is observed in all spectra at ≥150 °C. Its fraction increases steadily with temperature (Figure 10).

Along the heating path, the solution was supersaturated with respect to kieserite at elevated temperatures (probably at all $T > 100$ °C[3]). At 500 °C, the system moved towards equilibrium. Rapid growth of a kieserite crystal caused a simultaneous decrease in the $MgSO_4$ concentration in the fluid and thus in the intensity of the ν_1-SO_4^{2-} Raman band (Figure 11). At the same time, the quartz surface attained a corroded appearance and a new Raman band at 1053 cm^{-1} appeared in the spectra of the fluid. This peak position differs significantly (by +2 cm^{-1}) from that of the kieserite crystal at the same $P-T$ conditions (Figure 11a). This band cannot be explained by submicroscopic kieserite because Raman bands of nanocrystals are usually shifted to lower wavenumbers[41,42]. Therefore, this band is assigned to $\nu_s SO_3(HSO_4^-)$[43]. The Raman band at ~1050 cm^{-1} was only observed at the highest temperatures. Upon cooling, it disappeared from the spectra at $T > 300$ °C (Figure 11b).

From optical observations, the kieserite crystal still grew after cooling to 400 °C and dissolved at T≤300 °C. Further cooling to 22 °C did not result in complete dissolution. The existence of a kieserite solubility minimum between 300 and 400 °C is also indicated by the minimum in the integrated ν_1-SO_4^{2-} intensities in the Raman spectra of the fluid along the cooling path (Figure 11b). The concentration of $MgSO_4$ in the fluid at these conditions was estimated from the integrated intensities of the ν_1-SO_4^{2-} and the $\nu_s SO_3(HSO_4^-)$ Raman bands (Figure 11b) and their relative isotropic Raman scattering coefficients taken from Rudolph[43]. At the solubility minimum

the $MgSO_4$ molality in the fluid is reduced to about 0.4.

The large changes in the $MgSO_4$ concentration of the fluid along the cooling path imply considerable changes in the fluid density. Mass balance considerations lead to an estimate of about 1.24 g/cm^3 at 500 °C, 0.89 GPa after reaction to kieserite based on the determined $MgSO_4$ concentration in the fluid (0.85 molal) and a density of kieserite of 2.57 g/cm^3. Although molalities and densities differ from those of the heating path, the peak area fractions of the ν_1-SO_4^{2-} Raman band components show a very similar behavior (Figure 12). Likewise, a maximum of the 995 cm^{-1} component is observed at about 300 °C. The fraction of the 980 cm^{-1} component decreases and that of the 1005 cm^{-1} component increases with temperature. At the highest temperature (500 °C), the fraction of the HSO_4^- component is about 15%.

Discussion

Ab initio molecular dynamics simulations and Raman experiments are complementary approaches to study complexation and speciation in aqueous fluids. While the simulations provide direct access to individual species and can be performed at extreme $P-T$ conditions relatively easily, the constraints on accessible length and time scales make it difficult to obtain converged distributions of species. Moreover, the slowing down of particle dynamics with decreasing temperature may not even allow to reach equilibrium conditions at lower temperatures. In the present study, significant changes in speciation during the molecular dynamics runs were only observed at 727 °C and 527 °C. Thus, the results at lower T only provide trends under the assumption that the speciation does not change considerably with T. However, the low T runs were useful to evaluate the vibrational frequencies of individual species (Figure 6 and Figure 7) because the speciation changed much more frequently at high T. The Raman spectroscopic measurements, on the other hand, provide quantitative information on the distribution of different components to the studied vibrational mode from ambient to high P/T conditions. However, these components cannot be assigned unambiguously to the corresponding species without input from numerical modeling.

The most similar conditions of the simulations and the Raman experiments presented here were obtained at the highest temperature of the heating path before the precipitation of kieserite (2.2 molal solution, $T = 450$ °C, $\rho = 1.33$ g/cm^3) and the respective simulations of the 1.9 molal solution at $T = 527$ °C and $\rho = 1.35$ g/cm^3. At these conditions, the Raman spectra show roughly equal fractions of the three ν_1-SO_4^{2-} Raman band components at ∼980 cm^{-1}, ∼995 cm^{-1}, and ∼1005 cm^{-1}. The ν_1-SO_4^{2-} component at ∼995 cm^{-1} is usually assigned to CIPs, and the component at ∼980 cm^{-1} includes Raman-indistinguishable contributions from unassociated SO_4^{2-}(aq) ions, SIPs and 2SIPs[17]. As suggested by dielectric relaxation spectroscopy in $MgSO_4$ solutions to 65 °C[12], the fraction of 2SIPs and SIPs is strongly reduced with temperature. At the highest temperatures of our study, such species are most probably insignificant. The assignment of the third ν_1-SO_4^{2-} component at ∼1005 cm^{-1} is unsettled. This additional feature in the ν_1-SO_4^{2-} mode has also been observed at 23 °C in the Raman spectrum of a solution with a high Mg^{2+}/SO_4^{2-} ratio (4.098 molal $MgCl_2$+0.107 molal $MgSO_4$)[17]. It was interpreted as being due to the contact triple ion $Mg_2SO_4^{2+}$, based on results from dielectric relaxation spectroscopy[11] on concentrated $MgSO_4$ solutions, or to be related to bidentate CIP or larger complexes of Mg^{2+} and SO_4^{2-} [15,16].

The *ab initio* simulation results confirm most of the species previously suggested. In the high density range ($\rho > 1.2$ g/cm^3), fully hydrated SO_4^{2-}(aq), CIPs, triple ions and even larger complexes coexist on the picosecond time scale. In addition, monodentate and bidentate sulfate ligands are observed. This indicates that all of these species make a considerable contribution to the time averaged Raman spectrum. It also means that the number of sulfate species from *ab initio* calculations is much larger than that of Raman-distinguishable ν_1-SO_4^{2-} components. Unfortunately, the frequency resolution of the simulations is too low to assign individual species to spectral components. There is only the general trend that more associated species seem to have higher ν_1-SO_4^{2-} frequencies. This seems to be related to the slight deformation of the SO_4 tetrahedra, as shown in the Results section.

After nucleation and growth of kieserite, the fluid density decreased to about 1.2 g/cm^3, and the $MgSO_4$ concentration in the fluid to about 0.85 molal at 500 °C and 0.43 molal at 400 °C. At

these conditions, the Raman spectra of the fluid always showed an additional band at $\sim$1050 cm^{-1}, which is assigned to HSO_4^-, i.e. $\nu_s SO_3$ of this ion[43]. Formation of hydrogen sulfate ions shows that in addition to

$$Mg^{2+} + SO_4^{2-} = MgSO_4^0 \quad (1)$$

the reactions

$$Mg^{2+} + SO_4^{2-} + H_2O = MgOH^+ + HSO_4^- \quad (2)$$

and

$$SO_4^{2-} + H_2O = HSO_4^- + OH^- \quad (3)$$

take place and create buffer conditions. Even though the solution was significantly diluted due to formation of kieserite, comparison of the results from Raman spectroscopy and *ab initio* modeling is justified, because the changes in the sulfate speciation at constant P and T with $MgSO_4$ concentration are much larger in dilute solutions (< 0.25 molal) than at higher concentrations[17]. Indeed, HSO_4^-(aq) and $MgOH^+$(aq) are found in the simulations at fluid densities lower than 1.2 g/cm^3. The considerable shift in the vibrational frequencies of sulfur atoms in HSO_4^- towards higher values is also confirmed (Figure 7).

Raman spectroscopy in the ν_1(S-O) region is much more sensitive to the molecular environment of the sulfate molecule than the simulations. Since the number of components fitted to the spectra (three) is smaller than the likely number of frequent sulfate species, some of the highly associated species observed in the high $P-T$ fluid must have very similar vibrational properties. Similar behavior is observed at low P and T, where the component at $\sim$980 cm^{-1} includes Raman-indistinguishable contributions from unassociated SO_4^{2-}(aq) ions and the solvent-shared ion pairs SIPs and 2SIP[17]. This is because the first coordination shell of the sulfate in all these species is very similar, consisting only of water molecules. As an additional complication, the Raman spectra become very broad towards high temperatures, which may be due to thermal vibrations but also due to time averaging of dynamic changes in the speciation. Formation of hydrogen sulfate via bonding of a proton to one of the sulfate oxygens has a much stronger effect on the S-O vibrations

(bondlength, polarizability) than Mg-SO_4 association. This results in a considerably larger shift of the vibrational band towards higher wavenumbers.

Conclusions

Ab initio molecular dynamics simulations have provided new insight into the speciation in aqueous $MgSO_4$ fluids at high pressures and temperatures. From the results of this study, the Raman spectra of these fluids should be interpreted as follows. The ν_1-SO_4^{2-} Raman frequency of contact $MgSO_4$(aq) monomers or polymers in aqueous $MgSO_4$ solutions seems to depend on the number of Mg ligands of the sulfate and whether the Mg ligands are monodentate or bidentate. Both changes in the molecular environment of sulfate (two Mg ligands instead of one and bidentate instead of monodentate $MgSO_4$) appear to cause a shift of ν_1(S-O) towards higher wavenumbers and are not clearly distinguishable in the Raman spectra. Thus, the emergence of the component at $\sim$1005 cm^{-1} and the increase of its percentage with temperature only reflects increased ion association by both formation of more bidentate ligands and more polymers. In other words, the components at $\sim$995 cm^{-1} and $\sim$1005 cm^{-1} cannot be assigned to individual species (just as this is known to be the case for the $\sim$980 cm^{-1} ν_1-SO_4^{2-} component). Instead, they may be interpreted as a single 'Mg-SO_4 contact' component, with a frequency distribution depending on the type and number of Mg ligands of associated sulfate.

Acknowledgment

We are grateful to the *John von Neumann Institute for Computing* (NIC) Jülich for providing computing time on the IBM Blue Gene/L JUBL and on the IBM Blue Gene/P JUGENE. S.J. was supported by DFG project JA 1469/4-1.

References

(1) Newton, R. C.; Manning, C. E. *J. Petrol.* **2005**, *46*, 701–716.

(2) Philippot, P.; Selverstone, J. *Contrib. Mineral. Petrol.* **1991**, *106*, 417–430.

(3) Hogenboom, L.; Kargel, J. S.; Ganasan, J. P.; Lee, L. *Icarus* **1995**, *115*, 258–277.

(4) Chipera, S. J.; Vaniman, D. T. *Geochim. Cosmochim. Acta* **2007**, *71*, 241–250.

(5) McCord, T. B.; Hansen, G. B.; Fanale, F. P.; Carlson, R. W.; Matson, D. L.; Johnson, T. V.; Smythe, W. D.; Crowley, J. K.; Martin, P. D.; Ocampo, A.; Hibbitts, C. A.; Granahan, J. C.; the NIMS team, *Science* **1998**, *280*, 1241–1245.

(6) Hand, K. P.; Chyba, C. F. *Icarus* **2007**, *189*, 424–438.

(7) Noyes, A. A.; Melcher, A. C.; Cooper, H. C.; Eastman, G. W.; Kato, Y. *J. Am. Chem. Soc.* **1908**, *30*, 335–353.

(8) Ritzert, G.; Franck, E. U. *Ber. Bunsenges. Phys. Chem.* **1968**, *72*, 798–808.

(9) Tomšič, M.; Bešter-Rogač, M.; Jamnik, A.; Neueder, R.; Barthel, J. *J. Solution Chem.* **2002**, *31*, 19–31.

(10) Eigen, M.; Tamm, K. *Z. Elektrochem.* **1962**, *66*, 93–121.

(11) Buchner, R.; Chen, T.; Hefter, G. *J. Phys. Chem. B* **2004**, *108*, 2365–2375.

(12) Akilan, C.; Rohman, N.; Hefter, G.; Buchner, R. *ChemPhysChem* **2006**, *7*, 2319–2330.

(13) Davis, A. R.; Oliver, B. G. *J. Phys. Chem.* **1973**, *77*, 1315–1316.

(14) Rull, F.; Balarew, C.; Alvarez, J. L.; Sobron, F.; Rodriguez, A. *J. Raman Spectrosc.* **1994**, *25*, 933–941.

(15) Zhang, Y.-H.; Chan, C. K. *J. Phys. Chem. A* **2000**, *104*, 9191–9196.

(16) Zhang, Y.-H.; Chan, C. K. *J. Phys. Chem. A* **2002**, *106*, 285–292.

(17) Rudolph, W. W.; Irmer, G.; Hefter, G. T. *Phys. Chem. Chem. Phys.* **2003**, *5*, 5253–5261.

(18) Pye, C. C.; Rudolph, W. W. *J. Phys. Chem. A* **2001**, *105*, 905–912.

(19) Zhang, X.; Zhang, Y.; Li, Q. *J. Mol. Struc. (Theochem)* **2002**, *594*, 19–30.

(20) Zhang, H.; Zhang, Y.; Wang, F. *J. Comput. Chem.* **2009**, *30*, 493–503.

(21) Frantz, J. D.; Dubessy, J.; Mysen, B. O. *Chem. Geol.* **1994**, *116*, 181–188.

(22) Mancinelli, R.; Botti, A.; Bruni, F.; Ricci, M. A.; Soper, A. K. *J. Phys. Chem. B* **2007**, *111*, 13570–13577.

(23) Schmidt, C. *Geochim. Cosmochim. Acta* **2009**, *73*, 425–437.

(24) Hassan, S. A. *J. Phys. Chem. B* **2008**, *112*, 10573–10584.

(25) Sherman, D. M.; Collings, M. D. *Geochem. Trans.* **2002**, *3*, 102–107.

(26) Timko, J.; Bucher, D.; Kuyucak, S. *J. Chem. Phys.* **2010**, *132*, 114510.

(27) Hohenberg, P.; Kohn, W. *Phys. Rev.* **1964**, *136*, B864–B871.

(28) Kohn, W.; Sham, L. J. *Phys. Rev.* **1965**, *140*, A1133–A1138.

(29) Car, R.; Parrinello, M. *Phys. Rev. Lett.* **1985**, *55*, 2471–2474.

(30) Marx, D.; Hutter, J. Ab initio molecular dynamics: Theory and implementation. *Modern Methods and Algorithms of Quantum Chemistry, Forschungszentrum Jülich, NIC Series*, 2000; pp 301–449.

(31) Becke, A. D. *Phys. Rev. A* **1988**, *38*, 3098 – 3100.

(32) Lee, C.; Yang, W.; Parr, R. C. *Phys. Rev. B* **1988**, *37*, 785–789.

(33) Goedecker, S.; Teter, M.; Hutter, J. *Phys. Rev. B* **1996**, *54*, 1703–1710.

(34) Nosé, S.; Klein, M. L. *Mol. Phys.* **1983**, *50*, 1055–1076.

(35) Hoover, W. G. *Phys. Rev. A* **1985**, *31*, 1695 – 1697.

(36) Bassett, W. A.; Shen, A. H.; Bucknum, M.; Chou, I.-M. *Rev. Sci. Instrum.* **1993**, *64*, 2340–2345.

(37) Schmidt, C.; Ziemann, M. A. *Am. Mineral.* **2000**, *85*, 1725–1734.

(38) Everall, N. J. *Appl. Spectrosc.* **2000**, *54*, 773–782.

(39) Jahn, S.; Wunder, B. *Geochim. Cosmochim. Acta* **2009**, *73*, 5428–5434.

(40) Allen, M. P.; Tildesley, D. J. *Computer simulations of liquids*; Oxford University Press, 1987.

(41) Schmidt, C.; Rickers, K.; Wirth, R.; Nasdala, L.; Hanchar, J. M. *Am. Mineral.* **2006**, *91*, 1211–1215.

(42) Kostić, R.; Aškrabić, S.; Dohčević-Mitrović, Z.; Popović, Z. V. *Appl. Phys. A* **2008**, *90*, 679–683.

(43) Rudolph, W. W. *Z. Phys. Chem.* **1996**, *194*, 73–95.

Figures

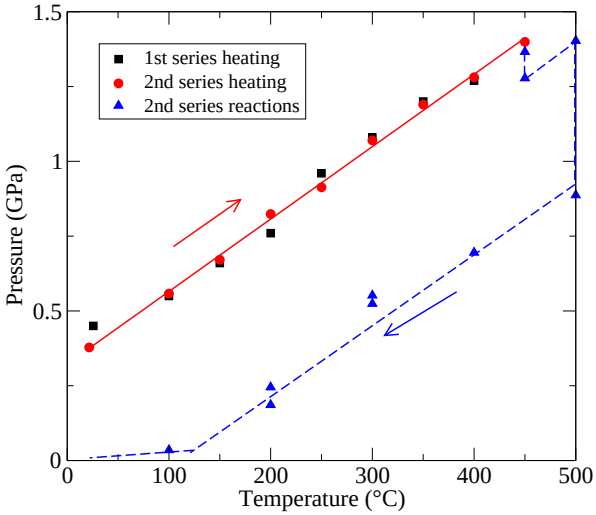

Figure 1: $P-T$ path of the experiments. The fluid density corresponding to the isochores of the heating cycles is 1.33 g/cm^3, whereas the fluid density after precipitation of kieserite is lowered to about 1.2 g/cm^3. Symbols indicate measured pressures from Raman spectra of quartz.

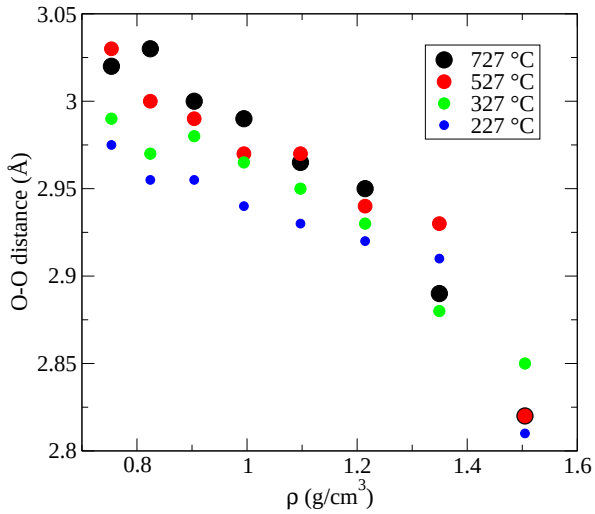

Figure 2: Nearest neighbor oxygen-oxygen distance as a function of temperature and fluid density. At all temperatures, the slope changes at densities in the range of 1.3±0.1 g/cm^3.

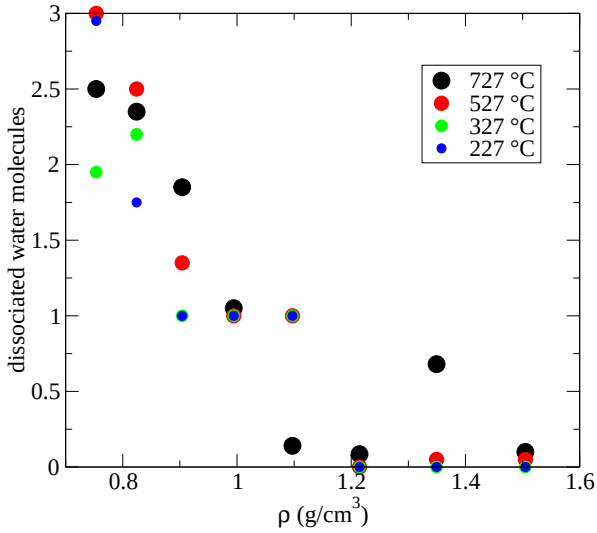

Figure 3: Time averaged number of dissociated water molecules (out of a total of 128) as function of fluid density. The released protons usually attach to the SO_4^{2-} molecules to form HSO_4^- bearing complexes.

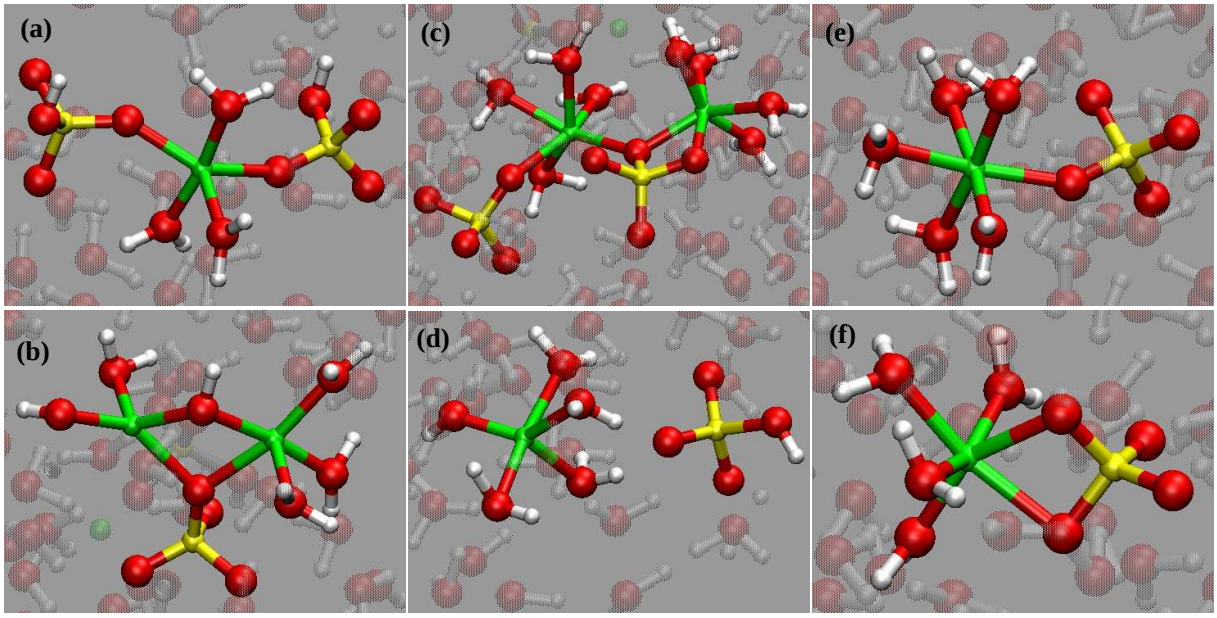

Figure 4: Snapshots from the simulations illustrating different species. Oxygens are represented as large red, Mg as green, S as yellow and H as white balls. Larger associated complexes such as triclusters, some of them containing additional protons or hydroxide ions, are dominant at low densities ($\rho = 0.75$ g/cm^3): $(HSO_4)Mg(HSO_4)$(aq) (a) and $(SO_4)(MgOH)_2$(aq) (b). Sometimes, association leads to the formation of short chains, e.g. of $MgSO_4MgSO_4$(aq) (c). Dissociated $MgOH^+$(aq) and HSO_4^-(aq) (d) are observed up to intermediate densities. At high densities, hydrolysis is suppressed, which leads to fully hydrated Mg^{2+}(aq) and SO_4^{2-}(aq) ions. Associated complexes at high density include monodentate (e) or bidentate (f) $MgSO_4$(aq) species but also larger clusters, such as triple ions or chains. Also noticeable is the increase of Mg coordination towards higher densities.

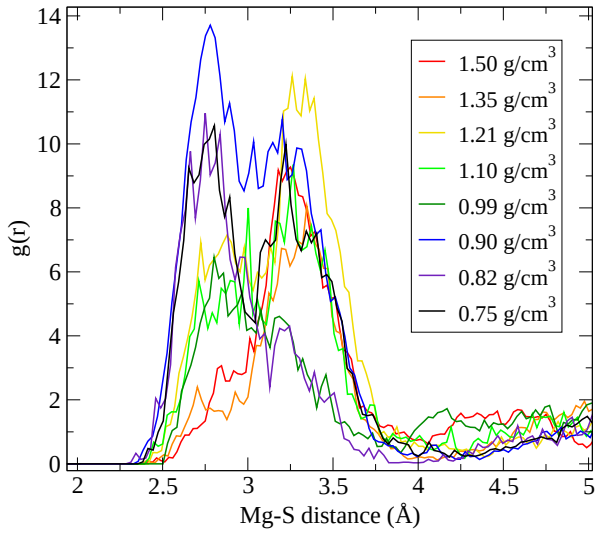

Figure 5: Mg-S radial distribution function at 727 °C. The peak around 3.3 Å is characteristic for a monodentate sulfate ligand whereas the peak around 2.8 Å represents the bidentate ligand.

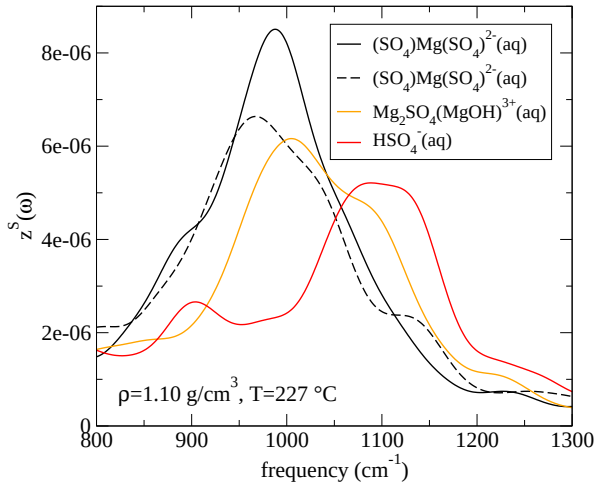

Figure 6: Example of vibrational spectra of the individual sulfur atoms at $T = 227$ °C and $\rho = 1.10$ g/cm^3 derived from the respective velocity autocorrelation functions. The two black lines correspond to sulfate groups bonded predominantly as monodentate ligands to a single Mg cation. The sulfate group represented by the solid black line also acted as bidentate ligand (40 % of the total simulation time). The yellow spectrum corresponds to a $Mg_2(SO_4)(MgOH)^{3+}$(aq) complex that was only observed at this density. The spectral weight of the HSO_4^-(aq) complex (red line) is clearly shifted to higher frequencies.

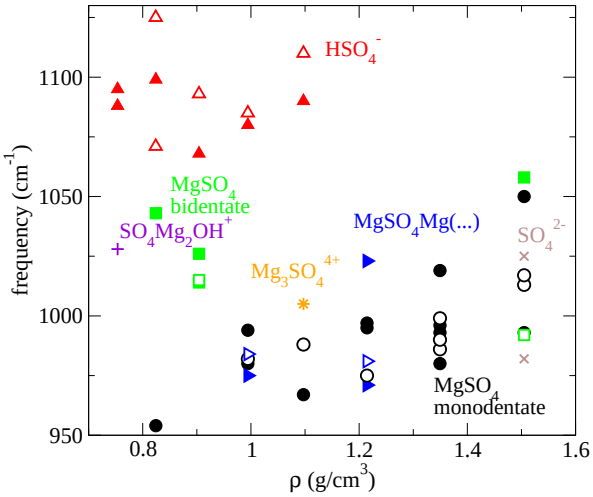

Figure 7: Vibrational frequencies of different sulfur atoms representing different sulfate species at 227 °C (filled symbols) and 527 °C (open symbols) as a function of density. The frequencies are obtained from the positions of the maxima of the respective vibrational spectra as shown, e.g., in Figure 6.

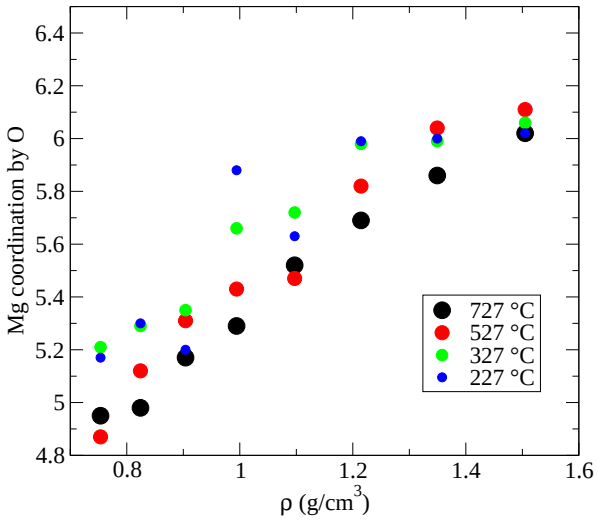

Figure 8: Average Mg coordination by oxygens as a function of temperature and fluid density.

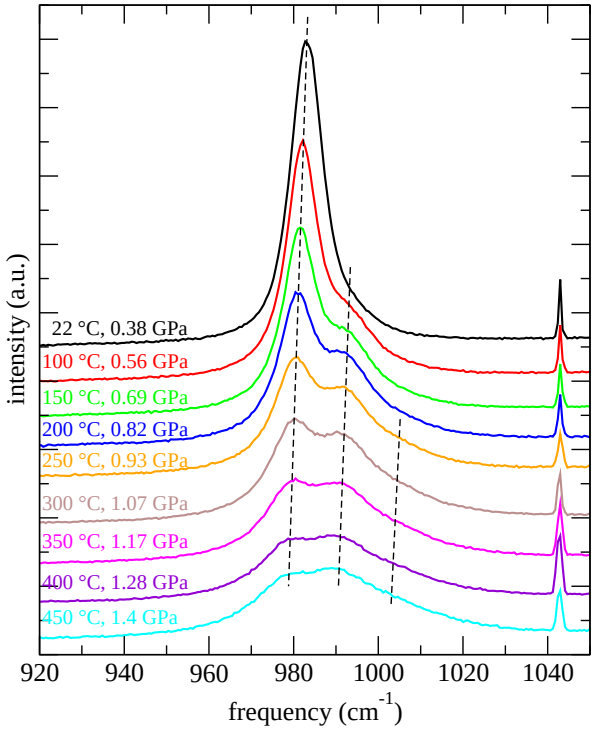

Figure 9: Raman spectra in the ν_1-SO_4^{2-} region of in the 2.2 molal $MgSO_4$ solution at isochoric $P-T$ conditions. Spectra are shifted along the intensity axis for clarity. The narrow line at 1044 cm^{-1} is a plasma line from the Ar^+ laser.

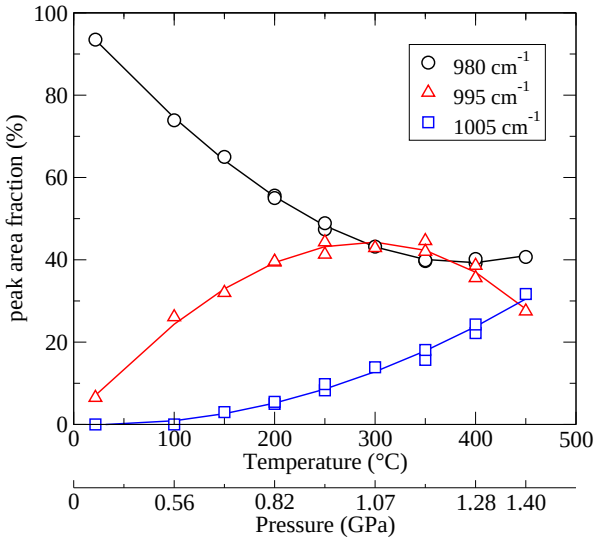

Figure 10: Relative integrated intensities of components of the ν_1-SO_4^{2-} Raman band in 2.2 molal $MgSO_4$ solution along the 1.33 g/cm^3 isochore.

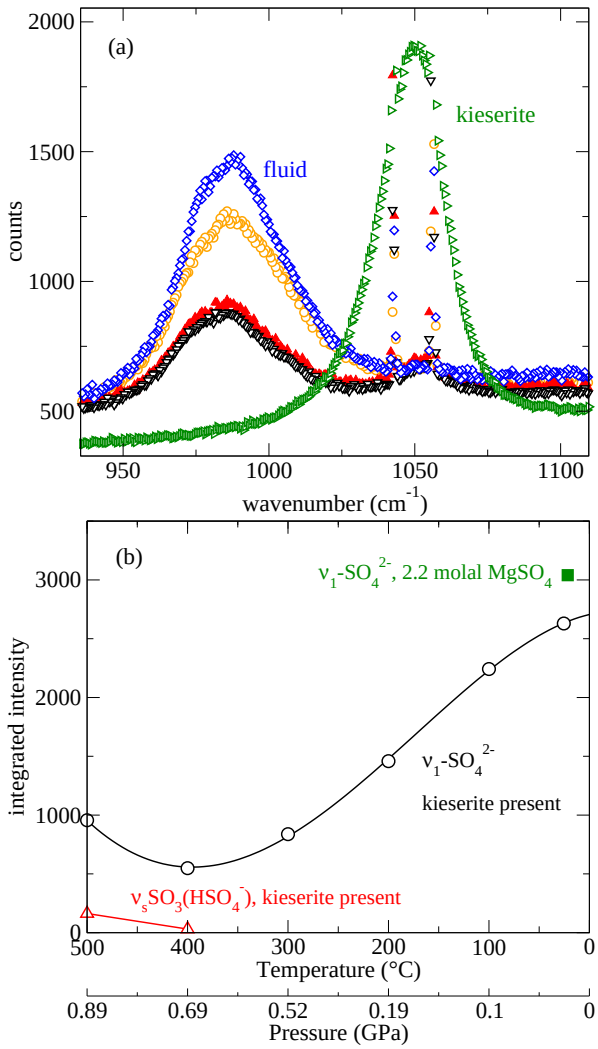

Figure 11: (a) Raman spectra in the ν_1-SO_4^{2-} and $\nu_s SO_3(HSO_4^-)$ region at 500 °C during kieserite crystal growth. Sequence of spectra (elapsed time after 500 °C were attained at $t = t_0$): blue, $t_0 + 5$ min; yellow, $t_0 + 10$ min; red, $t_0 + 20$ min; black, $t_0 + 25$ min. The green spectrum is that of the coexisting kieserite. Narrow lines at 1044 and 1057 cm^{-1} are plasma lines from the Ar^+ laser. (b) Integrated intensity of the ν_1-SO_4^{2-} and $\nu_s SO_3(HSO_4^-)$ Raman bands in the fluid in the presence of kieserite along the cooling path. Green square, solution at 0.38 GPa before heating.

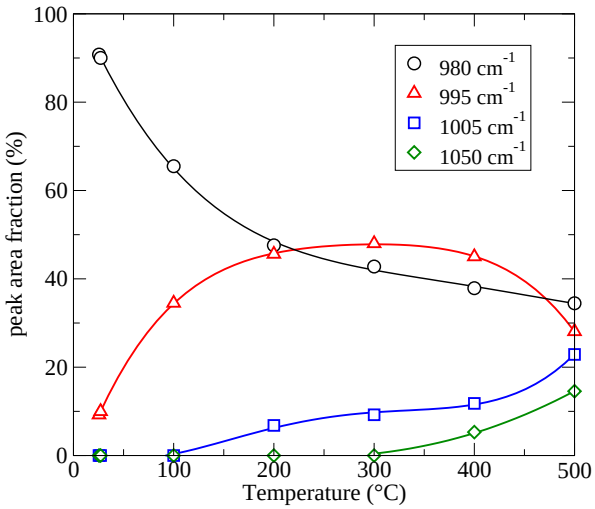

Figure 12: Relative integrated intensities of components of the ν_1-SO_4^{2-} Raman band in $MgSO_4$ solution along the cooling path ($MgSO_4$ molality variable).

Graphical TOC Entry